Macromolecules



pubs.acs.org/Macromolecules
Article

# Controllable Wet-Brush Blending of Linear Diblock Copolymers with Phenolic/DDSQ Hybrids toward Mesoporous Structure Phase Diagram

Ting-Chih Chou and Shiao-Wei Kuo*

Cite This: *Macromolecules* 2024, 57, 5958−5970
Read Online



**ABSTRACT:** In recent decades, the microphase separation behavior of diblock copolymers has been extensively discussed, whereby their inherent thermodynamic tendencies enable the bottom-up establishment of various self-assembled nanostructures. In this study, we employed ring-opening polymerization (ROP) to synthesize three linear poly(ethylene oxide-*b*-caprolactone) (PEO-*b*-PCL) diblock copolymers with different degrees of polymerization but similar volume fractions and utilized phenolic resin modified with double-decker silsesquioxane (PDDSQ) for controllable wet-brush blending. FTIR analyses revealed a competitive hydrogen bonding phenomenon and confirmed that increasing the chain length led to self-coiling of the segments, weakening the extent of hydrogen bonding. Through the evaporation-induced phase separation (EISA) mechanism, the cross-linking of PDDSQ, we obtained the mesoporous hybrid materials after template removal. Remarkably, through temperature-dependent SAXS, we were able to reproduce the changes in surface energy and *d*-spacing during the curing process of PDDSQ, demonstrating the mechanism of reaction-induced microphase separation leading to order−order phase transition. The presence of DDSQ resulted in a relatively higher $\chi$ value for the system, allowing for the formation of mesoporous structures such as lamella, hexagonal-packing cylinder, double gyroid, sphere, and even the less common hexagonal-perforated layer (HPL) structure. Additionally, the degree of polymerizations of the three diblock copolymers resulted in different $\alpha$ values ($\alpha = M_{n,h\text{-}A}/M_{n,b\text{-}A}$) for the blending system, whereby increasing the polymerization degree led to a decrease in the $\alpha$ value under the same blending weight fraction, prompting the system to form structures with higher interfacial curvature. TEM images and SAXS patterns served as evidence of this order−order phase transition. In summary, this study manipulated the polymerization degree of diblock copolymers to control the level of wet-brush blending in the system, presenting a mesoporous structure phase diagram for different weight fractions and template chain lengths, providing new insights and the opportunity to form desired self-assembled mesoporous structures at fixed volume fractions.

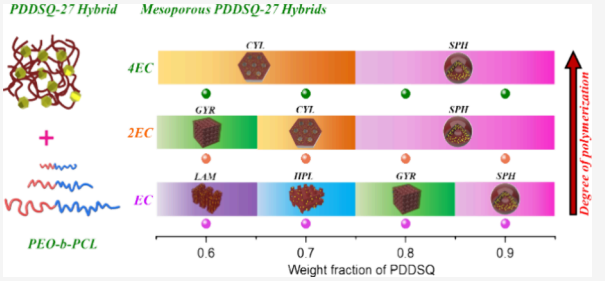




## INTRODUCTION

Self-assembled structures such as typical lamella (LAM), hexagonal packing cylinder (HPC), sphere, double gyroid (DG), and even special Frank−Kasper phases[1] of immiscible diblock copolymers (BCP) have been widely investigated during recent years because of their potential applications including soft lithography, photonic crystals, nanocomposites, and mesoporous materials.[2−7] The synthetic strategies of BCP with composition and structural variety are mainly from sequential addition of monomer through controlled living polymerization techniques or coupling reactions from the active chain ends with two different polymer chains.[8−11] It is well-known that the self-assembled structures are primarily dependent on the volume fraction, interaction parameter ($\chi$), and degree of polymerization ($N$); however, mediating the volume fraction is complicated and time-consuming through the controlled living polymerization.[12] As a result, blending homopolymer (A or B) into an A-*b*-B diblock copolymer is a relatively simpler method to mediate different self-assembled structures for varying volume fractions.[13]

In addition, the molecular weight of the homopolymer in A-*b*-B/A or A-*b*-B/B diblock copolymer/homopolymer blends strongly affects the self-assembled structures, including order−order morphological transition or macrophase separation, which is first proposed by Hashimoto and colleagues.[14] The $\alpha$ value ($\alpha = M_{n,h\text{-}A}/M_{n,b\text{-}A}$) is the ratio based on the molecular weight of the A segment in the homopolymer and the diblock copolymer that would have three different phenomena including (1) wet-brush behavior ($\alpha$ < 1), (2) dry-brush

Received: March 24, 2024
Revised: May 24, 2024
Accepted: May 26, 2024
Published: June 6, 2024

**Scheme 1. Chemical Structures of (a) PEO-*b*-PCL Diblock Copolymers with Various Chain Lengths and (b) PDDSQ-27 Hybrids and (c) the Phase Diagram of Mesoporous PDDSQ-27 Hybrids Templated by PEO-*b*-PCL Diblock Copolymers through EISA, Thermal Curing, and Pyrolysis**

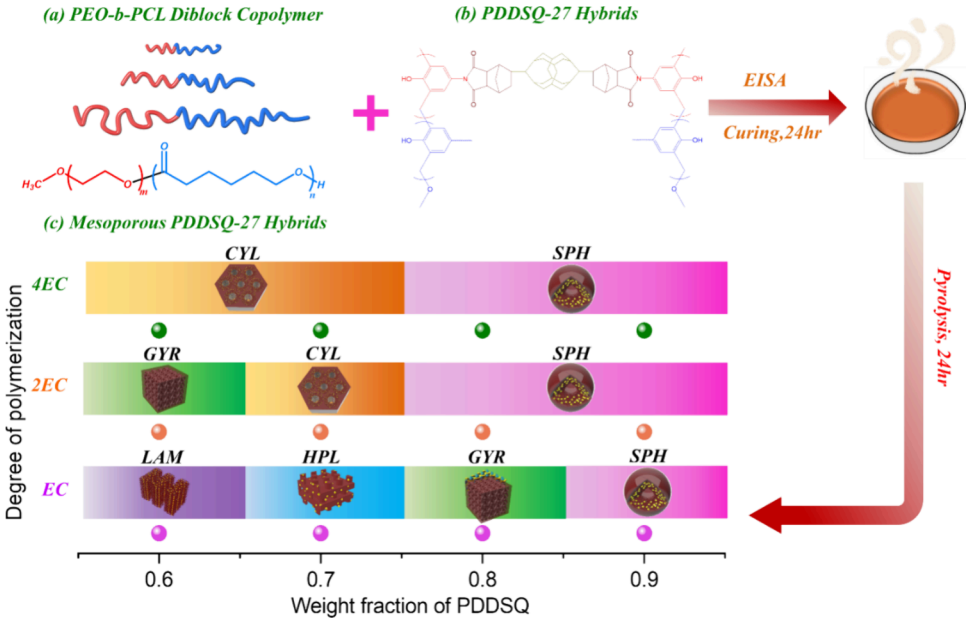


behavior ($\alpha$ = 1), and (3) total macrophase separation ($\alpha$ > 1).[14−17] The dry-brush behavior ($\alpha$ = 1) indicates that the self-assembled structures did not change through the addition of homopolymer into the diblock copolymer; however, a lower molecular weight of homopolymer A is miscible within the A block segment ($\alpha$ < 1), resulting in changes in domain sizes or even changes in self-assembled structures (order−order morphological transition), which is the "wet-brush" behavior.[15−17]

Recently, hydrogen bonding has been possible in diblock copolymer/homopolymer (A-*b*-B/C) blends[18−21] where the hydrogen bonding interaction of the C homopolymer with either the A or B block segment also undergoes the order−order morphological transition even if the molecular weight of the C homopolymer is larger than that of the corresponding block copolymer segment ($\alpha$ > 1), as determined by experimental or theoretical results.[22,23] As a result, the enthalpy term from the strong hydrogen bonding interaction of A/C or B/C binary blends could overcome the entropy term decrease from the higher molecular weight of the C homopolymer to provide the negative value of the Gibbs free energy. For example, Matsushita et al. used poly(styrene-*b*-2-vinylpyridine) (PS-*b*-P2VP, A-*b*-B) diblock copolymer blended with poly(vinylphenol) (PVPh, C) homopolymer where the PVPh/P2VP domain has strong intermolecular hydrogen bonding with microphase separation from the immiscible PS block segment.[24] They observed that the molecular weight of the C homopolymer strongly affects the self-assembled structures. At the same volume fraction of the PS block segment ($f_{PS}$ = 0.48), blending with a lower molecular weight PVPh homopolymer (8 or 14 kDa) formed an HPC structure; however, the higher molecular weight of PVPh (52 kDa) led to the LAM structure where the molecular weight of the P2VP block segment was 34 kDa. As a result, when $\alpha$ > 1, blending with 52 kDa PVPh homopolymer did not display macrophase separation, because the PVPh/P2VP domain had strong intermolecular hydrogen bonding and blending with the lower molecular weight PVPh homopolymer ($\alpha$ < 1); the chain conformation and the junction point distance were significantly influenced and thus have the better wet-brush behavior.[24]

During the past decade, the diblock copolymer/homopolymer blends mediated by hydrogen bonding strength have been widely used to synthesize mesoporous phenolic/silica materials.[25−30] For example, we used the poly(ethylene oxide-*b*-caprolactone) (PEO-*b*-PCL) diblock copolymers where the fixed molecular weight of PEO is 5 kDa as the template to prepare the mesoporous phenolic, silica, or phenolic/silica materials with DG, HPC, spherical, and Frank−Kasper phase structures based on the wet-brush behavior by mediating the competitive hydrogen bonding strength and block copolymer compositions.[31] Based on these previous studies, we have widely obtained the phase diagram of mesoporous phenolic, silica, and phenolic/double-decker silsesquioxane hybrid (PDDSQ hybrid) templated by the $PEO_{114}$-*b*-$PCL_x$ diblock copolymer with various degrees of polymerization of the PCL block segment.[32] However, in those previous studies,[31−34] the $\alpha$ value ($\alpha = M_{n,phenolic}/M_{n,PEO}$ or $M_{n,PDDSQ}/M_{n,PEO}$) is always constant for blend systems such as phenolic/$PEO_{114}$-*b*-$PCL_x$, TEOS/$PEO_{114}$-*b*-$PCL_x$, or PDDSQ/$PEO_{114}$-*b*-$PCL_x$. In this work, we have investigated the mesoporous PDDSQ hybrid phase diagram templated by different PEO-*b*-PCL diblock copolymers (nEC) with different degrees of polymerization of both PEO and PCL block segments, but the similar volume fractions of block copolymer segments through ring-opening polymerization required the addition of an equivalent amount of different molecular weights of poly(ethylene oxide) methyl ether ($M_n$ = 5, 10, and 20 kDa) and $\varepsilon$-caprolactone. Small angle X-ray scattering (SAXS) analyses provide the phase diagram, and the competitive hydrogen bonding interactions were characterized by Fourier transform infrared (FTIR) spectra within the PDDSQ/nEC blends. After the removal of nEC diblock copolymer templates, the mesoporous structures based on PDDSQ hybrids were characterized by using SAXS,


https://doi.org/10.1021/acs.macromol.4c00665
Macromolecules 2024, 57, 5958−5970

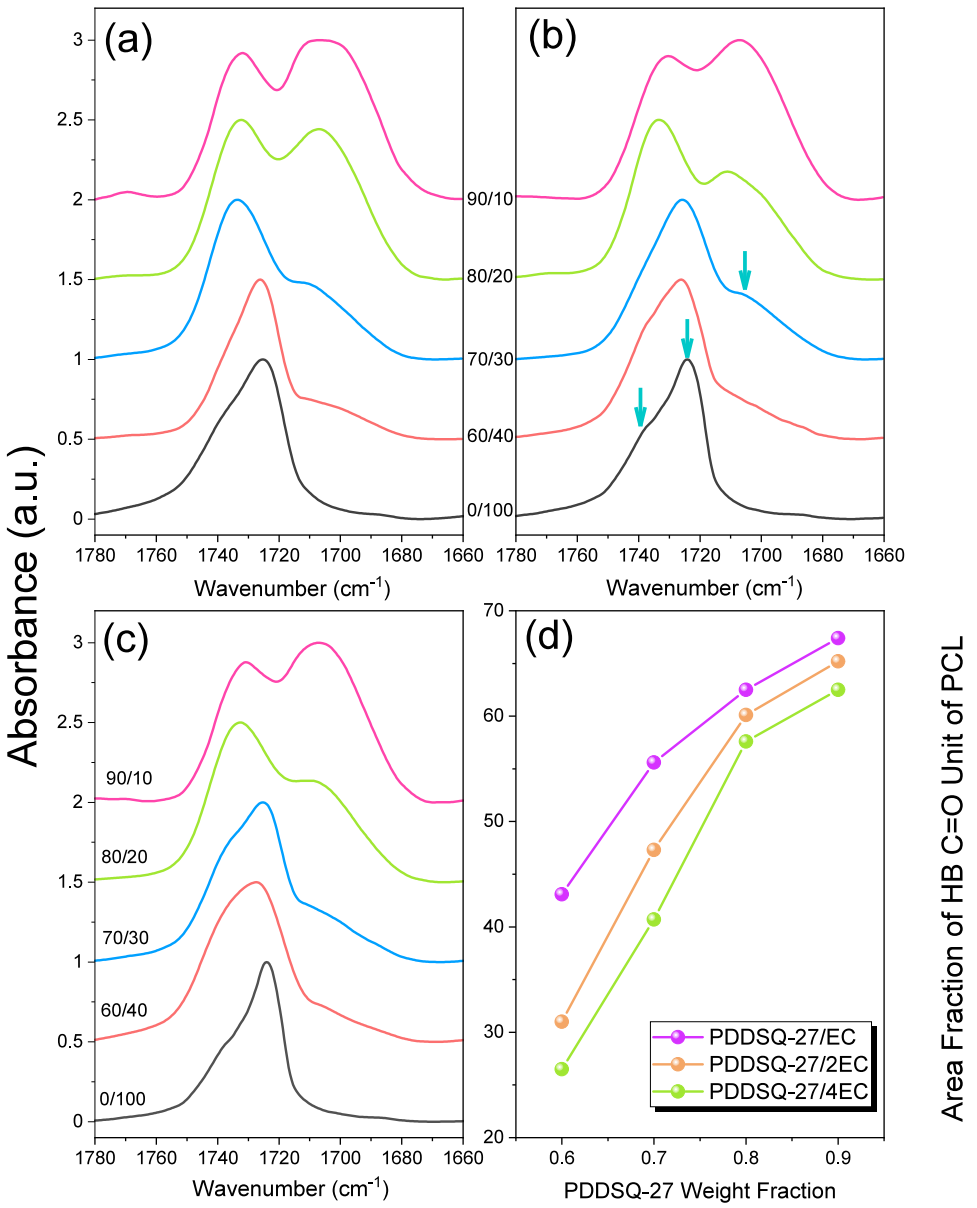


**Figure 1.** FTIR spectra of C═O regions recorded at room temperature of (a) PDDSQ-27/EC, (b) PDDSQ-27/2EC, and (c) PDDSQ-27/4EC blends and (d) the area fraction of hydrogen bonded C═O units of PCL segments of PDDSQ-27/nEC blends.

transition electron microscopy (TEM), and $N_2$ adsorption/desorption analyses. Overall, this work could provide the universal approach for the synthesis of mesoporous structures by varying the wet-brush behavior by mediating the $\alpha$ value with composition and competitive hydrogen bonding interaction.

## EXPERIMENTAL SECTION

**Materials.** The $\varepsilon$-caprolactone monomer and toluene underwent dehydration using $CaH_2$, which was sourced from Sigma-Aldrich. Chemicals such as 2-propanol, methanol, paraformaldehyde, tetrahydrofuran, acetonitrile, toluene, ethyl acetate, dimethylformamide (DMF), 1,4-dioxane, hydrochloric acid, and hexane were obtained from J. T. Baker. Dichloromethane and tin(II) 2-ethylhexanoate were procured from Alfa Aesar. Various PEO-*b*-PCL diblock copolymers with different degrees of polymerization but similar volume fractions (Scheme 1a; FTIR, GPC, and $^1$H and $^{13}$C NMR analyses in Figure S1) were prepared by ring-opening polymerization involving the addition of an equivalent amount of different molecular weights of poly(ethylene oxide) methyl ether ($M_n$ = 5, 10, and 20 kDa) and $\varepsilon$-caprolactone. A phenolic/DDSQ (PDDSQ) hybrid containing 27 wt % DDSQ (Scheme 1b; FTIR in Figure S2) was produced through the step-growth reaction involving DDSQ-4OH, phenol, and paraformaldehyde in an alkaline setting.[35,36] Composition of PEO-*b*-PCL diblock copolymers, polydispersity indices (PDI), and molecular weights (abbreviated as nEC diblock copolymer; 2EC has nearly two times the molecular weight for both segments compared to EC) are summarized in Tables S1. The molecular weight of the PDDSQ-27 hybrid was 4450 Da based-on GPC analysis, and the preparation route was demonstrated in Scheme S1.[31,35,36]

**Preparation of PPDSQ/nEC Blends and Mesoporous PDDSQ Hybrids.** The PDDSQ hybrid was synthesized by regulating the concentration ratio between DDSQ-4OH (POSS framework) and phenol (resin branches). Specifically, the weight fraction of DDSQ was maintained at 27 wt % in the PDDSQ matrix used in this study. Diblock copolymers of PEO-*b*-PCL (nEC) with varying molecular weights were prepared at a fixed volume fraction of $f_{PEO}$ = 0.32. To dissolve blends of PDDSQ/nEC with different ratios, tetrahydrofuran (THF) was employed, after which the solutions were transferred to an


https://doi.org/10.1021/acs.macromol.4c00665
Macromolecules 2024, 57, 5958−5970

aluminum pan. Evaporation-induced self-assembly (EISA) was carried out by gradually evaporating the solvent at 35 °C over a span of 36 h. A thermal treatment at 150 °C for 12 h facilitated the cross-linking of the phenolic groups, thereby solidifying the microstructure. Subsequently, by subjecting the blends to temperatures exceeding the pyrolysis threshold of 350 °C for 12 h, the diblock copolymer was eliminated, leaving behind self-assembled PDDSQ mesoporous hybrids (Scheme 1c). Finally, a heating process at 800 °C for 6 h within a tube furnace under a nitrogen atmosphere resulted in the formation of mesoporous PDDSQ carbon materials.

## RESULTS AND DISCUSSION

**FTIR, SAXS, and TEM Analyses of PDDSQ-27/nEC Blends.** In our previous studies, we extensively investigated the hydrogen bonding interactions between the OH functional groups of phenolic resin or PDDSQ hybrid and the ether groups in the PEO block as well as the carbonyl groups in the PCL block. In this study, our emphasis is on discussing the influence of altering the overall degree of polymerization ($N$) of these diblock copolymers on the hydrogen bonding interactions within the PDDSQ blending system, and the induced structural formations. In Figure S3, upon analyzing the FTIR spectra of PDDSQ-27/nEC blends, a signal is observed at 3385 $cm^{-1}$, corresponding to the self-association hydrogen bonding unit of the pure PDDSQ-27 hybrid in the OH stretch region. With the incorporation of the various nEC diblock copolymers, the self-association hydrogen bond shifts to a lower wavenumber, specifically to 3240 $cm^{-1}$, as the concentration of nEC increases. This phenomenon arises due to the pronounced manifestation of the OH−ether hydrogen bond at relatively lower PDDSQ concentrations.[37−40] Conversely, at higher PDDSQ concentrations, hydrogen bonds could concurrently form within both the PEO and the PCL segments. This phenomenon explains the FTIR spectra of lower PDDSQ concentrations presenting a plateau-like curve, indicating that the OH stretch signal arises from the superposition of peaks originating from distinct positions. The intermolecular association constants ($K_A$) for the phenolic/PEO and phenolic/PCL blends are determined to be 264 and 116, respectively.[37−39] Such closely aligned values instigate competitive phenomena within the system when altering the concentration of the hydrogen bond donor, PDDSQ, as extensively discussed in prior literature. At elevated PDDSQ concentrations, hydrogen bonds are established in both the PEO and PCL block regions. Conversely, under lower PDDSQ concentrations, preferential interactions are observed to occur predominantly with the PEO block.

It is noteworthy that, through the analysis of the C═O groups in PCL segments, multiple peaks are observed in the C═O region due to the establishment of hydrogen bonds facilitated by the presence of phenolic OH functional groups, as displayed in Figure 1. In the FTIR spectra, pure nEC diblock copolymers exhibit two absorption bands at 1734 and 1724 $cm^{-1}$, respectively, corresponding to the free (amorphous) and crystalline C═O groups.[37−40] Upon increasing the concentration of PDDSQ-27 to 60 wt % and analyzing the spectra through curve fitting (Figure S4), in addition to the original peaks, new absorption peaks appear at 1706 $cm^{-1}$ for blends with varying chain lengths, PDDSQ-27/EC (Figure 1a), PDDSQ-27/2EC (Figure 1b), and PDDSQ-27/4EC (Figure 1c), these peaks signify the presence of C═O units influenced by intermolecular hydrogen bonding. As the concentration of PDDSQ-27 rises to 70 wt %, PCL's crystalline peak vanishes for PDDSQ-27/EC and remains for 2EC and 4EC blends. This phenomenon could be explained by the self-screening effect introduced by the chain length. As the degree of polymerization increases, the segments have a higher chance of self-coiling, limiting their contact with the functional groups and reducing the number of formed hydrogen bonds with the PDDSQ.[38,40] The weaker hydrogen bonds between PDDSQ and PCL prevent the disruption of crystalline regions in the C═O units of 2EC and 4EC. Consequently, we observe the persistence of peaks at 1724 $cm^{-1}$ in the FTIR spectra. When the concentration of PDDSQ-27 exceeds 80 wt %, all crystalline C═O units are disrupted due to the formation of hydrogen bonds with PDDSQ. Consequently, all block copolymers with varying degrees of polymerization exhibit only two distinct C═O peak values, corresponding to the amorphous phase (free) and the hydrogen bonding influenced PCL. Additionally, the fraction of hydrogen bonds under different blending ratios could be similarly identified through FTIR curve fitting. By analyzing the proportion of peak areas in FTIR attributed to C═O units influenced by hydrogen bonding (Figure 1(d)), we can elucidate factors influencing the fraction of hydrogen bonds. As depicted in Figure 1(d), an increase in the concentration of PDDSQ-27 provides opportunities for hydrogen bond formation of the PCL block segment. The phenomenon of self-coiling brought about by longer chain segments results in a lower fraction of hydrogen bonded C═O units of the PCL block segment under conditions of equal PDDSQ-27 concentration compared to shorter chain segments. Furthermore, this result can also be explained by the higher molecular weight of the PEO block segment; the OH units of the PDDSQ hybrid predominantly interact with the PEO block segment rather than the PCL block segment, and thus the lower $\alpha$ value ($\alpha = M_{n,PDDSQ}/M_{n,PEO}$) would reduce the fraction of hydrogen bonded C═O units of the PCL block segment. A lower $\alpha$ value also indicates the wet-brush behavior would have an easy order−order morphological transition compared with results at a higher $\alpha$ value as expected.[15−17]

Besides, Figure S5 focuses on the C−O−C stretch of the PEO segment in the wavenumber range 1260−1170 $cm^{-1}$, presenting the situation of different weight fractions of PDDSQ/nEC room temperature blending samples. As an example, for the pure diblock copolymer template (0/100), there are two peaks in this range at wavenumbers 1243 and 1190 $cm^{-1}$, representing the crystalline peaks of PEO itself. With the introduction of PDDSQ, hydrogen bonds disrupt crystallization, causing the peak at 1243 $cm^{-1}$ to broaden and the crystalline peak at 1190 $cm^{-1}$ to disappear. Through peak fitting, a new peak appears at 1223 $cm^{-1}$, representing the C−O−C stretch affected by hydrogen bonding, causing the adjacent crystalline peak at 1243 $cm^{-1}$ to broaden or even form a plateau. From the FTIR information, as shown in Figure S5, with the increase in chain length, the peak intensity of PEO crystallization shows an increasing trend for samples with the same blending ratio, especially for samples with blending ratios of PDDSQ/nEC = 80/20 and 70/30, where the growth of the crystalline peak (1190 $cm^{-1}$) and the weakening of the C−O−C peak affected by hydrogen bonding (1223 $cm^{-1}$) are particularly noticeable. This phenomenon could also be attributed to the self-coiling phenomenon caused by elongation of the chain length. The increased length of the PEO segment makes it more prone to coiling and crystallizing. At the same time, the chance of hydrogen bonding with the ether functional group of PEO decreases, as evidenced by


https://doi.org/10.1021/acs.macromol.4c00665
Macromolecules 2024, 57, 5958−5970

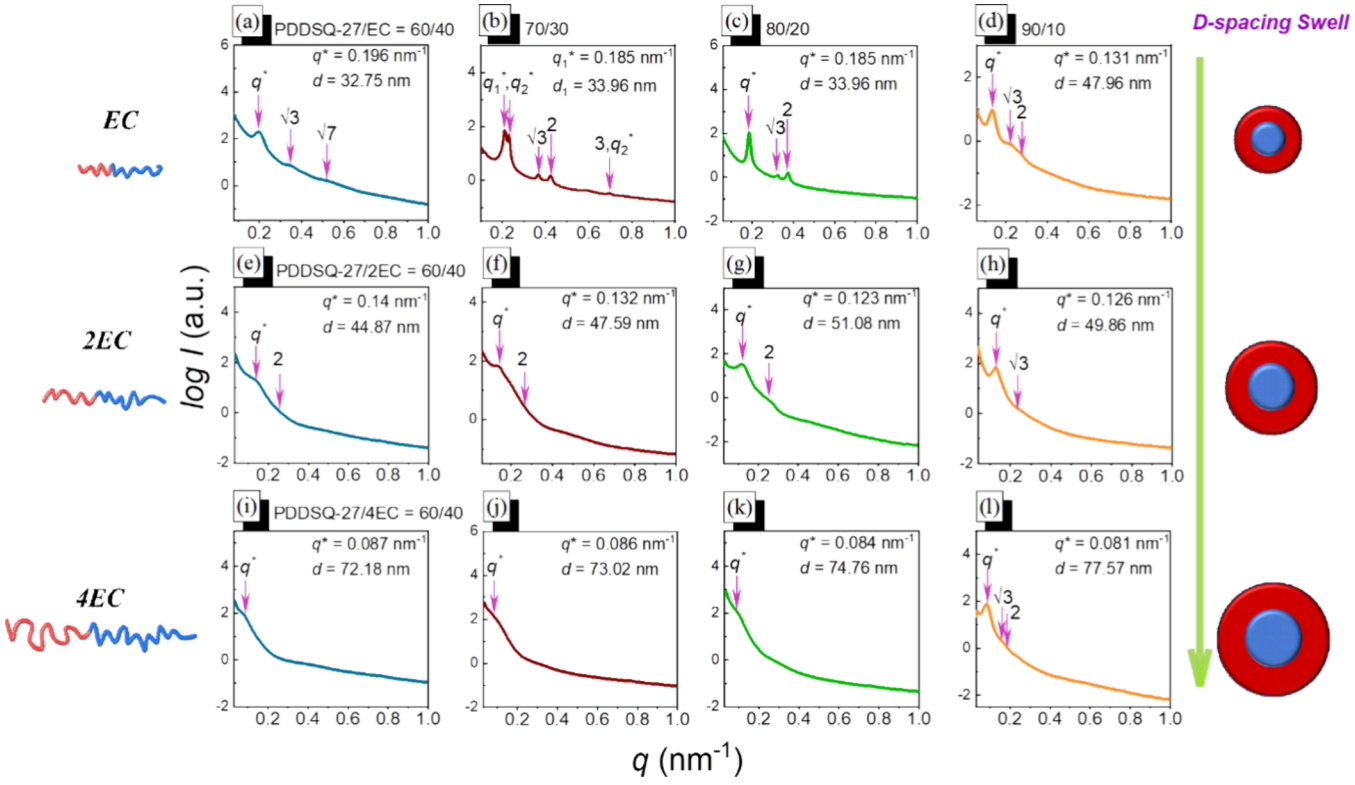


**Figure 2.** SAXS analyses of (a−d) PDDSQ-27/EC blends, (e−h) PDDSQ-27/2EC blends, and (i−l) PDDSQ-27/4EC blends with various compositions.

FTIR analysis, explaining the fluctuation between the hydrogen bonded C−O−C functional group and PEO crystallization with the increase in the chain length.

Now, we magnify the observation on the scale from atom to mesophase, where the hydrogen bonding and evaporation-induced self-assembly (EISA) affect polymer chains collaboratively, arranging them into specific geometry structures. To characterize the self-assembled structures of PDDSQ-27/nEC blends after EISA, we performed SAXS analyses on samples under different conditions, as shown in Figure 2 at room temperature. Based on Figure 2(a)−(d), starting with the shortest EC diblock copolymer, the PDDSQ-27/EC = 60/40 blend has a hexagonal packing cylinder structure, with characteristic $q$ ratios of $1:\sqrt{3}:2:\sqrt{7}$. As the concentration of PDDSQ-27 reaches 70 wt %, some intriguing findings are revealed in the SAXS patterns. Two first-order $q^*$ peaks are labeled as $q_1^*$ and $q_2^*$; this phenomenon is owing to the coexistence of two structures, a hexagonal packing cylinder and lamella. As we could observe, the relative spacing of $q_1^*/q = 1:\sqrt{3}:2$ and $q_2^*/q = 1:2:3$ is consistent with our assumption. This complex spacing ratio is distinctive and first discovered in the phenolic/EC binary blend system. For the PDDSQ-27/EC = 80/20 blend, the sharp peaks with $q$ ratios of $1:\sqrt{3}:2$ prove the existence of the cylinder structure. As the concentration increases to 90 wt %, the morphology switches to sphere structure, which is similar to all high phenolic concentration blend samples.[31−35]

When the chain length of the template is doubled, the regularity of the PDDSQ-27/2EC blend samples decreases, as evidenced by the broadening and fuzziness of the SAXS peaks. We regard that, under the conditions of a chain length of 2EC, all PDDSQ-27 samples with concentrations ranging from 60 to 80 wt % exhibit a short-range ordered cylinder structure, while samples with a concentration of 90 wt % exhibit a spherical structure, as presented in Figure 2(e)−(h). As mentioned previously,[32] the increase in the $N$ value of block copolymer chains leads to self-coiling, which weakens hydrogen bonding with the PCL segment. This also signifies a decrease in the driving force for microphase separation in the self-assembly system, ultimately preventing the ideal formation of self-assembled structures. This explains why, as the lengths of block copolymer chains increase, the phase separation of the formed structures becomes less clear. Similarly, PDDSQ-27/4EC blending samples have one spherical micelle for the 90/10 blend and three disorder structures for the 80/20, 70/30, and 60/40 blends, as shown in Figure 2(i)−(l). Additionally, we notice that, at the same volume fraction, increasing the $N$ values from EC to 4EC will lower the $q^*$ value and enlarge the $d$-spacing. When the PDDSQ-27 concentration is fixed at 90 wt %, from EC to 2EC to 4EC, domain size is broadened from 47.96 to 49.86 to 77.57 nm. The variation of the $d$-spacing implies that a higher degree of polymerization can affect the intermolecular interaction and inflate the microphase separation region further. The result of short-range ordered structure from PDDSQ-27/4EC = 80/20, 70/30, and 60/40 is due to the level inflation exceeding the tolerance range of the forming condition of the self-assembled structure.

What is even more remarkable is that the mixed samples of the PDDSQ-27/EC = 70/30 blend at room temperature exhibit a unique complex dual-peak combination, simultaneously featuring distinct first-order $q^*$ peaks for both lamella and hexagonal packing cylinder structures. Hence, we are curious to explore how the reaction-induced changes in chain segments within the system would influence the alterations in the self-assembled structures. The variable temperature SAXS patterns have done an excellent job of showcasing changes in


https://doi.org/10.1021/acs.macromol.4c00665
Macromolecules 2024, 57, 5958−5970

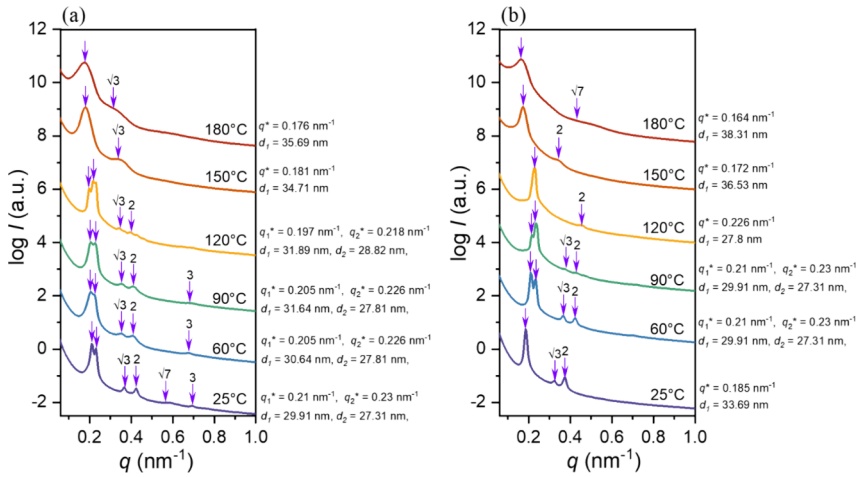


**Figure 3.** Variable temperature SAXS patterns for (a) PDDSQ-27/EC = 70/30 and (b) PDDQ-27/EC = 80/20 blends.

morphologies and *d*-spacing upon heating to 180 °C. PDDSQ-27 phenolic resin has a relatively high POSS concentration, and thus, the blending system has a high $\chi$ value. According to self-consistent field theory (SCFT),[41−43] a system that has a high $\chi$ value belongs to a strong segregation region. Thus, a high $\chi$ value will make the self-assembled structure more distinct. Moreover, when the $\chi N$ value belongs to the low part of strong segregation region (usually high $\chi$ and low $N$), sophisticated architecture such as double gyroid and hexagonal-perforated layer could be found. As displayed in Figure 3(a), by checking the SAXS peaks of the PDDSQ-27/EC = 70/30 blend, we could obtain two sets of $q^*/q$ ratios: $q_1^*/q$ = 1:$\sqrt{3}$:2:$\sqrt{7}$ and $q_2^*/q$ = 1:3, where $q_1^*/q$ has the ratio of cylinder and larger *d*-spacing and $q_2^*/q$ has the ratio of lamella and smaller *d*-spacing. As the temperature rises, during the 60−120 °C interval, we could clearly observe that the intensity of $q_1^*$ declines, while the intensity of $q_2^*$ increases, and other peaks become obscure as well. We consider this phenomenon to be caused by reaction-induced microphase separation and interfacial energy decrease due to the melting behavior ($T_m$ = 60−70 °C) of PEO and PCL blocks and the vanishing of hydrogen bonds under rising temperatures.[44−47] Based on thermodynamic theory, when the interfacial energy decreases, the self-assembly micelle tends to increase its interfacial surface area in order to minimize the Gibbs free energy. Thus, the phase transition from the lamella/cylinder mixture to lamella occurs because of the higher surface area of the lamella structure. When the temperature reaches 150 °C, the peaks of the lamella disappear and the structure transforms to pure hexagonal packing cylinder. This second phase transition is owing to the surface energy enhancement again; once the thermal curing process of PDDSQ propagates, especially over 120 °C, it is cross-linked with a high rigid structure. As a result, the interfacial surface energy rises again. Besides, the *d*-spacing increases along with the formation of the cross-linked network structure of PDDSQ-27, from 27.31 to 35.69 nm. We also discuss the SAXS patterns of the PDDSQ-27/EC = 80/20 blend, as shown in Figure 3(b). The room temperature sample has hexagonal packing cylinder characteristic $q$ ratios of 1:$\sqrt{3}$:2, and 60−120 °C intervals have the first-order phase transition from cylinder to lamella. The languishing of the cylinder's $q^*$ peak and rising of the lamella's $q^*$ peak and the two $q^*$ peak coexisting situations at 60 °C are evidence of phase transition. The second phase transition happened at 150 °C, in which two different blending ratios have identical temperatures. Lamella structure switches back to cylinder can be identified by the rapid shrinking of the $q^*$ value and the characteristic $q^*$ ratio of 1:$\sqrt{3}$:$\sqrt{7}$ at 180 °C. Variation of *d*-spacing is abnormal; from room temperature, we have 33.69 nm with the cylinder structure. During the first phase transition, the appearance of the lamella structure makes the *d*-spacing decrease, and not until the second phase transition does the *d*-spacing rise again to 38.31 nm with the emergence of the cylinder structure. These two high $\chi$ blending samples have clear order−order phase transition behavior and are sensitive to the variation of interfacial energy, indicating that, when the PDDSQ blended systems are heated, all of them could be affected by this phenomenon but to different degrees.[31,32,47]

In the temperature-dependent FTIR analysis, we could observe the changes in the state of the blend and discuss the mechanism of the reaction-induced phase separation. Figure S6 presents the variable temperature FTIR analysis in the C═O stretch region for the blend ratio of PDDSQ-27/4EC = 70/30. Similar to variable temperature SAXS, recordings were taken every 30 °C starting from room temperature. In the graph, we observe that, at 30 °C, the overall signal comprises three overlapping peaks, representing amorphous PCL at 1734 cm$^{-1}$, crystalline PCL at 1724 cm$^{-1}$, and PCL affected by a H bond at 1706 cm$^{-1}$. As the temperature rises to 60 °C, exceeding the $T_m$ of PCL, all peaks located at 1724 cm$^{-1}$ shift to 1734 cm$^{-1}$ due to the melting of crystalline PCL. This phenomenon indicates a change in the microstructure under heating and explains why a phase transition occurs in variable temperature SAXS when the temperature reaches 60 °C. As the temperature continues to rise, the peak at 1706 cm$^{-1}$ gradually weakens, indicating a decrease in the strength of hydrogen bonds between PCL and PDDSQ-27. We believe that this change stems from two reasons. First, an increase in temperature is unfavorable for the stability of hydrogen bonds, leading to a decrease in the overall hydrogen bond strength between PDDSQ-27 and PEO-*b*-PCL. Second, upon heating, cross-linking decreases the concentration of −OH functional groups, and since PEO has an association constant ($K_A$) higher than that of PCL, −OH groups in the blend system gradually transfer from the PCL domain to PEO, prioritizing hydrogen bond formation with PEO, thereby reducing the hydrogen bond strength of PCL. From Figure S6,


https://doi.org/10.1021/acs.macromol.4c00665
Macromolecules 2024, 57, 5958−5970

we observe that this weakening of hydrogen bonds is consecutive and increases with temperature, which can explain the reason for the phase transition observed in SAXS analysis above 60 °C.

**Mesoporous PDDSQ Hybrid Materials Templated by EC Diblock Copolymers.** After thermal curing, we used a pyrolysis temperature of 400 °C for PEO-*b*-PCL and then obtained mesoporous PDDSQ-27 hybrid materials. In this section, mesoporous samples with different blending conditions are introduced. First, we used SAXS patterns to display the phase transition of morphologies before and after thermal calcination. Fixing the blending ratio at 60 wt % PDDSQ-27, SAXS stacking patterns of PDDSQ-27/EC and PDDSQ-27/2EC blends are shown in Figure 4(a),(b), respectively. The PDDSQ-27/EC blend has a cylinder structure after thermal curing, and removing the EC diblock copolymer makes the morphology transform to a lamella structure with classical $q^*/q$ = 1:2:3 ratios, as displayed in Figure 4(a). PDDSQ-27/2EC exhibits disordered micelle structure after thermal curing and becomes a double gyroid structure with peak ratios of $\sqrt{2}:\sqrt{6}:\sqrt{8}:\sqrt{16}:\sqrt{22}:\sqrt{50}$ after removal of the 2EC template, as shown in Figure 4(b). Here, we observed the appearance of a peak at the $\sqrt{2}$ position, which is absent in the typical double gyroid structure. The emergence of this peak can be attributed to the deformation of the double gyroid structure, where two coherent networks undergo deformation after the removal of the PEO-*b*-PCL template. This alteration breaks the inversion symmetry of the double gyroid phase, resulting in SAXS patterns resembling those of the single gyroid phase.[48,49]

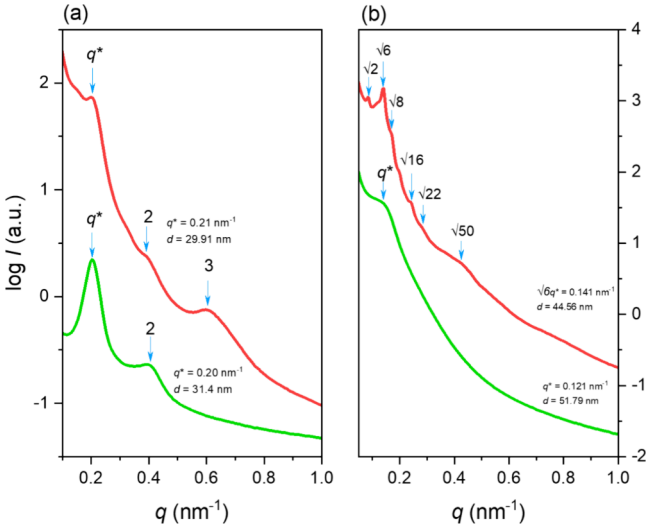


**Figure 4.** SAXS patterns of (a) PDDSQ-27/EC = 60/40 and (b) PDDSQ-27/2EC = 60/40 blends before (green line) and after (red line) thermal pyrolysis at 350 °C.

Herein, we could discover the *d*-spacing diminishes in both chain lengths, from 31.4 to 29.91 nm and 51.79 to 44.56 nm from PDDSQ-27/EC = 60/40 and PDDSQ-27/2EC = 60/40 samples. When the template is removed, the PDDSQ region loses the support, and therefore, the *d*-spacing shrinks. Moreover, since the temperature is high during the thermal calcination, the PDDSQ shell might distort slightly; two effects collaborate to give the opportunity for phase transition to happen. In Scheme 2, we have an illustration of self-assembled structures of PDDSQ-27/nEC = 60/40 blends (Scheme 2(a)), depicting the variation of morphologies after EISA, thermal curing (Scheme 2(b)), and template pyrolysis (Scheme 2(c)), respectively. For each thermal treatment, PDDSQ blending with EC, 2EC, and 4EC templates is arrayed from the bottom to the top; the growth size of the model structures also indicates the increase in the degree of polymerization and *d*-spacing.

Figure 5 shows the self-assembled mesoporous structures with different blending ratios templated by the shortest EC chain based on TEM images, SAXS patterns, and $N_2$

**Scheme 2. Mesoporous PDDSQ-27 Hybrids (a) from Self-Assembled Structure of PDDSQ-27/nEC = 60/40 Blends, (b) after EISA and Thermal Curing, and (c) from Template Pyrolysis Mediated by Different Chain Lengths of PEO-*b*-PCL Diblock Copolymers**

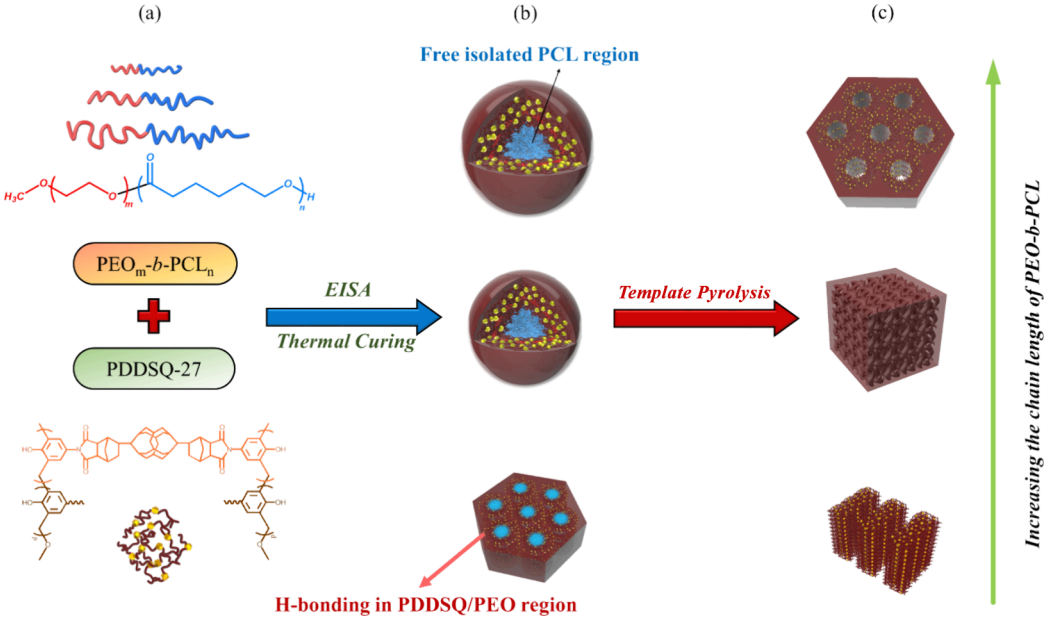




https://doi.org/10.1021/acs.macromol.4c00665
Macromolecules 2024, 57, 5958−5970

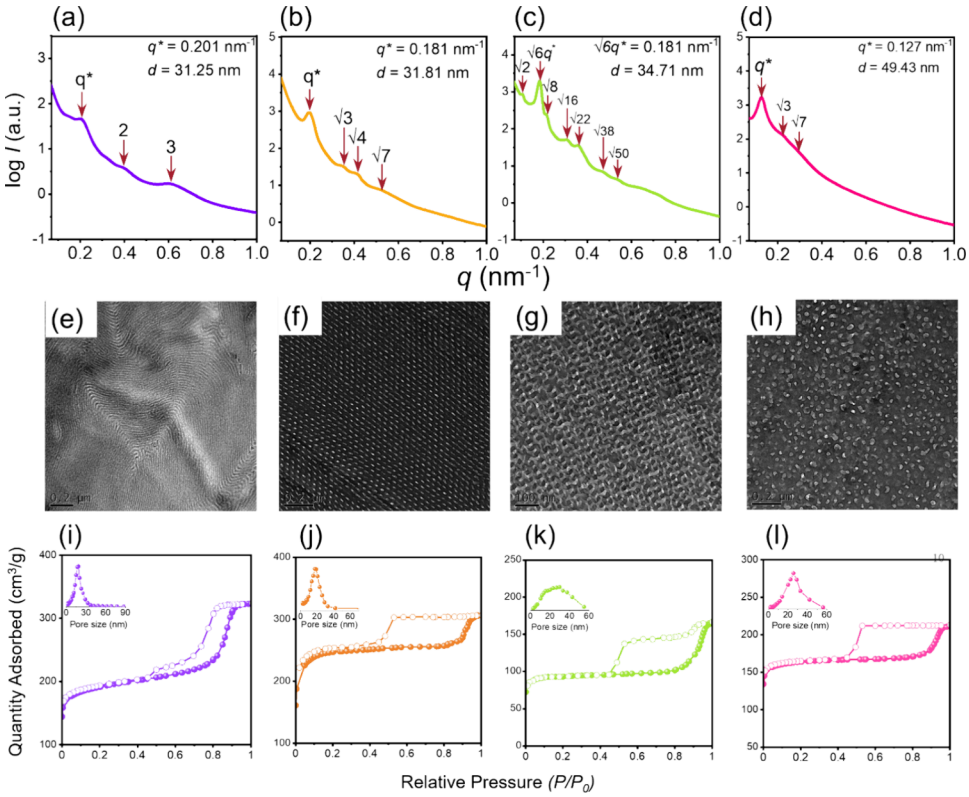


**Figure 5.** (a–d) SAXS measured at room temperature and (e–h) TEM images and (i–l) $N_2$ sorption/desorption isotherms and pore size distribution for mesoporous PDDSQ hybrids at 77 K templated from PDDSQ-27/EC of (a, e, i) 60/40, (b, f, j) 70/30, (c, g, k) 80/20, and (d, h, l) 90/10 blends.

adsorption/desorption analyses. A long-range order lamella structure is formed when the concentration of PDDSQ-27 is 60 wt %; SAXS patterns with peak ratios of 1:2:3 as shown in Figure 5(a) and the TEM image in Figure 5(e) with black and gray strip packing alternately could also be evidence. $N_2$ adsorption/desorption isotherms recorded at 77 K are displayed in Figure 5(i), revealing the typical type IV(a) curve, with a value of $P/P_0$ from 0.4 to 0.8 for the capillary condensation step. $H_5$ hysteresis loops are specified, representing the existence of both blocked and partially opened mesopores within the slightly collapsed layered structure, and the mean pore size was 18.9 nm calculated from the Harkins and Jura model,[39] as shown in the inset of Figure 5(i). Figure 6(b) is the TEM image of the B projection surface from the [100] direction, which has an alternating black strip and another black strip with equidistance rectangular pores; every two adjacent strips that have rectangular pores possess staggered arrangement, which is due to the perforation being staggered between two neighbor layers. Clean lamella projection is obtained and represents the projection image from the C direction, which can prove the presence of an alternating layer, denoted as C, as shown in Figure 6(c). In Figure 6(d), we captured the projection of the B and C surface interface, where the upper one is the [100] plane and the lower one is the [010] plane, where two surfaces are separated well and arranged reasonably. The SAXS pattern displays the $q^*/q = 1:\sqrt{3}:\sqrt{4}:\sqrt{7}$ peak ratios, which could prove the existence of the hexagonal-perforated layer (HPL) structure indirectly in Figure 5(b), both the characteristic ratios of lamella and cylinder are detected without any miss. The PDDSQ-27/EC = 80/20 blend has a long-range order double gyroid phase.

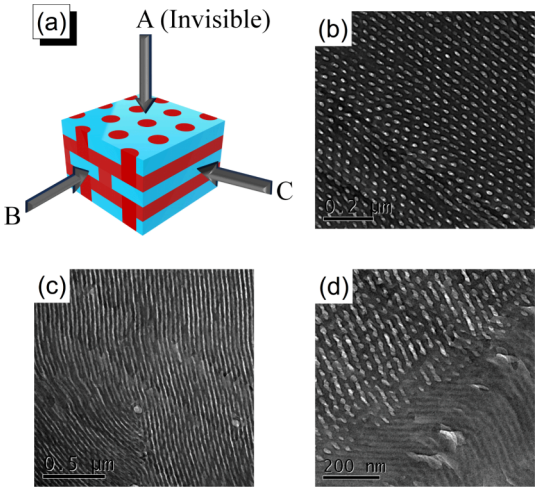


**Figure 6.** (a) Schematic representation of the HPL morphology and its cross-sectional pattern from different Miller indices. TEM images of the mesoporous PDDSQ hybrid from PDDSQ-27/EC = 70/30 blend that has the same packing order as the projection of (b) B, [100] direction, (c) C, [010] direction, and (d) interface of B and C, [110] direction.

Figure 5(g) is the TEM image of the (111) projection surface. Besides, SAXS patterns (Figure 5(c)) with characteristic ratios of $\sqrt{2}:\sqrt{6}:\sqrt{8}:\sqrt{16}:\sqrt{22}:\sqrt{38}:\sqrt{50}$ could be compelling evidence of the existence of the double gyroid structure. Finally, this blending system ends up with normal spherical mesoporous structure (Figure 5(d),(h)), based on SAXS and TEM analyses, when the PDDSQ-27 concentration is 90 wt %. Figure 5(i)–(l) shows that $N_2$ adsorption/desorption


https://doi.org/10.1021/acs.macromol.4c00665
Macromolecules 2024, 57, 5958–5970

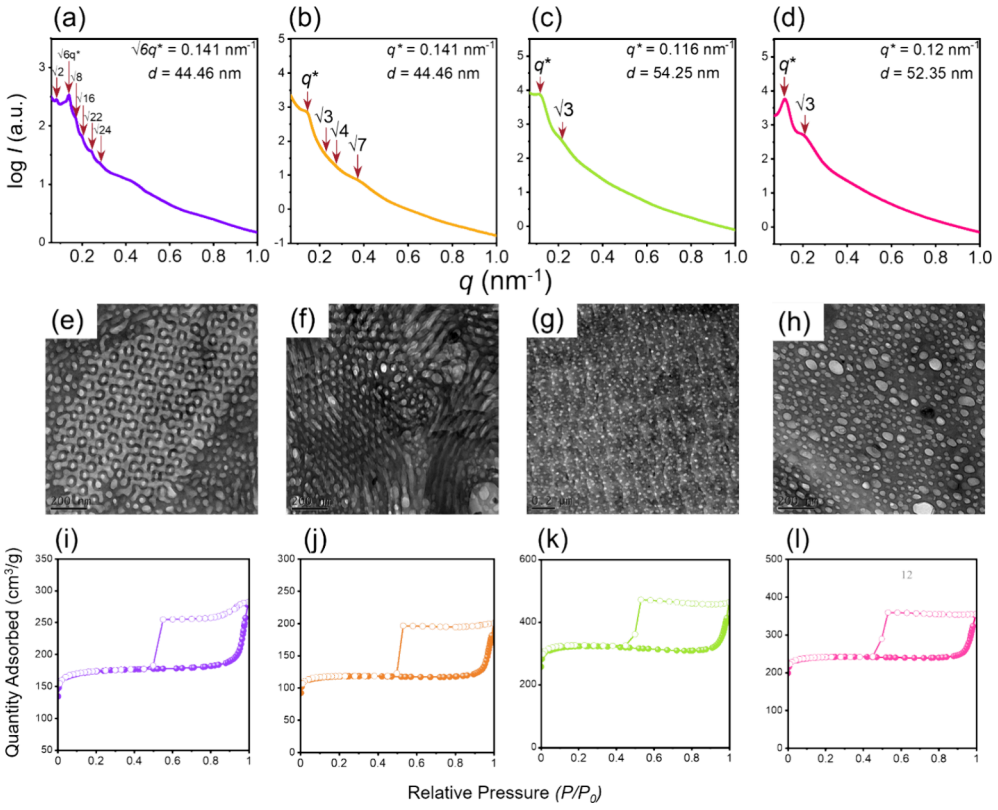


**Figure 7.** (a–d) SAXS measured at room temperature and (e–h) TEM images and (i–l) $N_2$ sorption/desorption isotherms for mesoporous PDDSQ hybrids at 77 K templated from PDDSQ-27/2EC of (a, e, i) 60/40, (b, f, j) 70/30, (c, g, k) 80/20, and (d, h, l) 90/10 blends.

isotherms of mesoporous PDDSQ hybrids from PDDSQ-27/EC = 70/30, 80/20, and 90/10 blends have typical type IV(a) curves, and their capillary condensation steps occur at $P/P_0$ from 0.8 to 0.95; $H_1$ hysteresis loops are observed from 0.4 to 0.9, 0.45 to 0.95, and 0.45 to 0.95, implying the existence of long-range order cylindrical pores or double gyroid structures in mesoporous scale, and the pore size curves are also displayed as insets with each isotherm.

The degree of polymerization of the entire PEO-*b*-PCL block copolymer was doubled, and PDDSQ mesoporous hybrid materials were prepared by using 2EC as the template. The SAXS, TEM, and $N_2$ adsorption/desorption analyses for different blending ratios are presented in Figure 7. In Figure 7(a), SAXS peak ratios are observed as $\sqrt{2}:\sqrt{6}:\sqrt{8}:\sqrt{16}:\sqrt{22}:\sqrt{24}$, corroborated by the TEM projection image in Figure 7(e), confirming the presence of a double gyroid structure in the mesoporous PDDSQ hybrid from the PDDSQ-27/2EC = 60/40 blend. Increasing the PDDSQ-27 concentration to 70 wt % led to the emergence of hexagonally packing cylinder structures, validated by the TEM image and SAXS peak ratio of $1:\sqrt{3}:\sqrt{4}:\sqrt{7}$ (Figure 7(b),(f)). For PDDSQ-27 concentrations exceeding 80 wt %, SAXS peak ratios of $1:\sqrt{3}$ were observed (Figure 7(c),(d)), and TEM analyses (Figure 7(g),(h)) indicated the spherical micelle structure. Mesoporous PDDSQ-27 materials templated by 2EC exhibited similar nitrogen adsorption–desorption isotherms across different ratios, all belonging to type IV(a), with $H_1$ hysteresis types, as displayed in Figure 7(i)–(l).

Figure 8 consolidates all SAXS, TEM, and $N_2$ adsorption–desorption analyses for blends of PDDSQ-27 with the longest 4EC chains at various weight ratios. According to Figure 8(a),(b), the SAXS peak ratios of mesoporous PDDSQ hybrids from PDDSQ-27/4EC = 60/40 and 70/30 blends are both $1:\sqrt{3}:\sqrt{4}:\sqrt{7}:\sqrt{9}$, indicating the HPC structure. However, TEM images in Figure 8(e),(f) reveal some irregularities in this HPC structure. This irregularity can be attributed to the self-coiling phenomenon mentioned earlier, where the highest molecular weight of 4EC tends to self-coil in the system, making hydrogen bonding less likely to occur. As shown in Figure 1(d), 4EC has the lowest proportion of hydrogen bonded C═O units among all segments, especially when the concentration of PDDSQ-27 is low. Consequently, these long PCL segments may not be adequately restrained by PDDSQ-27, leading to disordered self-assembled structures, resulting in overexpanded mesopores or irregular arrangements. When the weight percentage of PDDSQ-27 exceeds 80 wt %, spherical micelle structures become the only self-assembled structures, as evidenced by the $1:\sqrt{3}$ peak ratios in Figure 8(c),(d) and TEM images in Figure 8(g),(h). Similar to PDDSQ-27/2EC, nitrogen adsorption–desorption isotherms of mesoporous PDDSQ hybrids from the PDDSQ-27/4EC samples all belong to type IV(a), with $H_1$ hysteresis loops indicating pronounced mesopore filling delays.

Additionally, by fixing the weight ratio of PDDSQ-27 and PEO-*b*-PCL and focusing on observing the effects of increasing the template's degree of polymerization, we obtained a captivating phase transition phenomenon. Figure S7(a) shows the SAXS patterns of the mesoporous samples from PDDSQ-27/nEC = 60/40 blends. We obtained the lamella structure from the PDDSQ-27/EC sample, mentioned in the last paragraph. As the template doubles the chain length from EC to 2EC, a double gyroid complex structure is formed, which is verified by SAXS peak ratios. It is the first time we have discovered the phenolic resin-based hybrid materials with


https://doi.org/10.1021/acs.macromol.4c00665
Macromolecules 2024, 57, 5958–5970

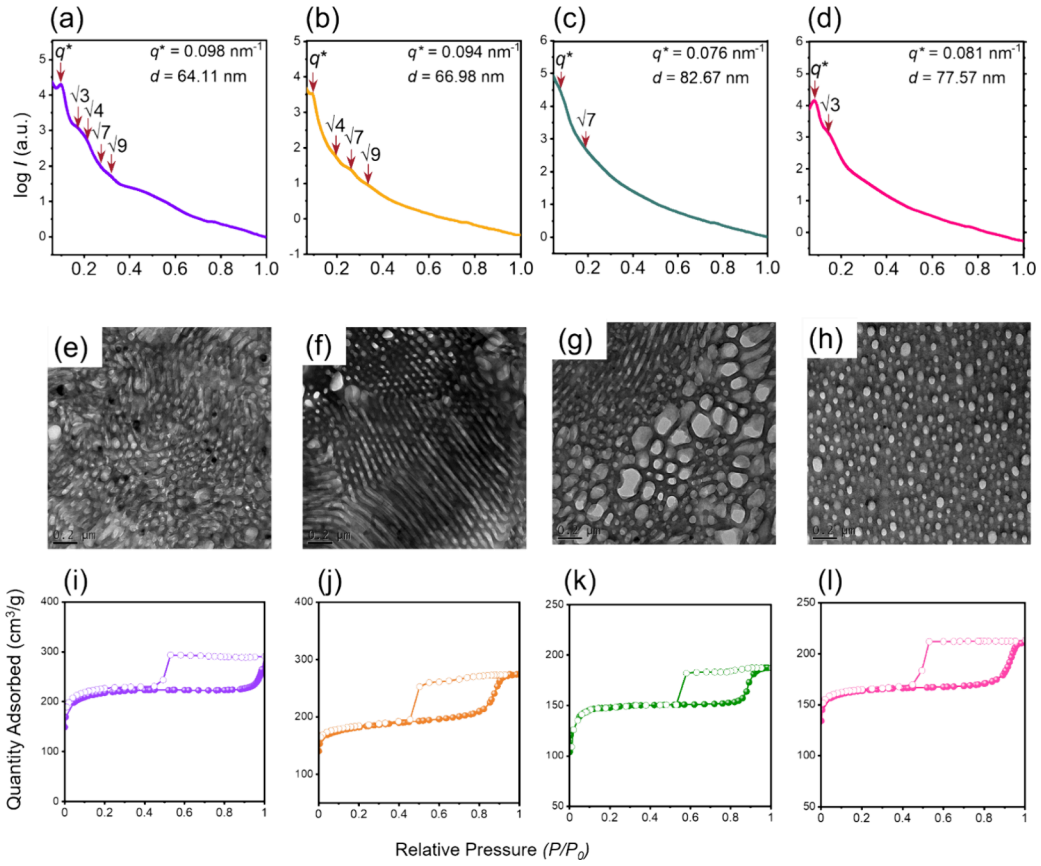


**Figure 8.** (a–d) SAXS measured at room temperature and (e–h) TEM images and (i–l) $N_2$ sorption/desorption isotherms for mesoporous PDDSQ hybrids at 77 K templated from PDDSQ-27/4EC of (a, e, i) 60/40, (b, f, j) 70/30, (c, g, k) 80/20, and (d, h, l) 90/10 blends.

a double gyroid structure in a high degree of polymerization condition; normally, this complex structure tends to form at high $\chi$ and low $N$ and transforms to pure cylinder or lamella as the $N$ value increases.[13−16,41,50−52] Once the chain length goes up to 4EC, we obtain a slightly irregular HPC structure. To explain the mechanism for this phase transition caused by an increase of the degree of polymerization, a significant idea needs to be elaborated, the wet-brush behavior of the blending system and the screening effect of hydrogen bonding. In Scheme 2, the PEO-*b*-PCL diblock copolymer has phase separation and is split into two domains. After blending with the PDDSQ-27 hybrid, the hydrogen bonding between PEO and PDDSQ-27 will make them stick together, and because the molecular weight of PDDSQ-27 is smaller than PEO's, it will be dissolved in PEO chains and inflate the domain (brown region); this phenomenon is also called wet brush. As the degree of polymerization increases, 2EC has 2 times molecular weight and chain length compared to EC, but the same volume fraction for PEO and PCL block segments. Since the molecular weight of the PDDSQ-27 remains unchanged, $\alpha_{2EC}$ is smaller than $\alpha_{EC}$, this means that the level of wet brush is higher when the molecular weight of diblock copolymers increases. Thus, PDDSQ-27/4EC has the greatest wet-brush condition, and PDDSQ-27 are well dispersed in the PEO domain. We consider that the level of wet brush is the indicator of the tendency for chains to stretch. If we have two phase separation cases with identical volume fractions, one consists of long blocks (PCL) and the other consists of long blocks and short chains in the wet-brush condition (PDDSQ-27 and PEO). The wet-brush one has higher conformational entropy loss owing to the swells of the microdomain and the stretch of the chains. Therefore, when the level of wet brush increases, the entropic penalty becomes dominant, surpassing the enthalpic penalty, raising the interfacial curvature between two domains. Conclusively, the degree of polymerization increase will enlarge the chain length difference between PDDSQ-27 and block copolymers, and the wet-brush domains are prone to stretch and swell, leading to larger interfacial curvature. With this idea, we could understand why LAM transforms to DG and why DG transforms to cylinder (CYL) structure when the chain length increases because of the rising of interfacial curvature. The model structures are displayed in Scheme 2(c). Besides, it is worth mentioning that *d*-spacing rises obviously from 31.25 to 44.46 to 64.11 nm as the chain length increases, which is derived from the elongation of the template causing the micelle to enlarge. For mesoporous materials, the larger size of a micelle is equivalent to a bigger pore size; therefore, the *d*-spacing is increased when the degree of polymerization is raised.

When the PDDSQ-27 concentration is increased to 70 wt %, HPL is formed from the PDDSQ-27/EC = 70/30 blend, as explained in the previous paragraph. As the chain length rises, both 2EC and 4EC samples are cylinder structures, verified by the SAXS curve presented in Figure S7(b). Similarly, the phase transition of PDDSQ-27/nEC = 70/30 blends occurs toward the increase of interfacial curvature, consistent with the enhancement of the wet-brush level. The *d*-spacing was increased from 31.73 to 45.86 to 67.56 nm from EC to 2EC to 4EC, respectively. Table 1 summarizes the BET information for all of the mesoporous PDDSQ hybrids. Based on this data,


https://doi.org/10.1021/acs.macromol.4c00665
Macromolecules 2024, 57, 5958−5970

**Table 1. Mesoporous PDDSQ-27 Hybrids Templated by nEC Diblock Copolymers from SAXS and $N_2$ Sorption/Desorption Isotherm Analyses**

| Samples | *d*-spacing (nm) | $S_{BET}$ ($m^2$/g) | $S_M$ ($m^2$/g) | Pore volume ($cm^3$/g) | Pore size (nm) |
|---|---|---|---|---|---|
| **PDDSQ-27/EC = 6/4** | 31.25 | 432 | 382 | 0.071 | 18.9 |
| **PDDSQ-27/2EC = 6/4** | 44.46 | 535 | 447 | 0.157 | 27.1 |
| **PDDSQ-27/4EC = 6/4** | 64.11 | 642 | 580 | 0.216 | 51.1 |
| **PDDSQ-27/EC = 7/3** | 31.81 | 327 | 299 | 0.086 | 15.9 |
| **PDDSQ-27/2EC = 7/3** | 45.86 | 359 | 319 | 0.126 | 25.6 |
| **PDDSQ-27/4EC = 7/3** | 67.56 | 487 | 446 | 0.198 | 44.6 |
| **PDDSQ-27/EC = 8/2** | 34.71 | 280 | 261 | 0.093 | 17.8 |
| **PDDSQ-27/2EC = 8/2** | 52.35 | 881 | 783 | 0.217 | 26.5 |
| **PDDSQ-27/4EC = 8/2** | 66.98 | 911 | 865 | 0.237 | 58.9 |
| **PDDSQ-27/EC = 9/1** | 49.43 | 501 | 432 | 0.068 | 14.4 |
| **PDDSQ-27/2EC = 9/1** | 54.25 | 609 | 471 | 0.114 | 39.7 |
| **PDDSQ-27/4EC = 9/1** | 71.31 | 733 | 663 | 0.169 | 42.1 |

several conclusions could be drawn. First, through the TEM images and BET pore size information provided in the preceding paragraphs, we could confirm that the pores of all samples in this study belong to the mesoporous scale (2−50 nm). Second, as we increase the degree of polymerization of the template, the pore size and surface area of the mesoporous materials will definitely increase. Additionally, we observed that, under the same template molecular weight, the surface area of DG, LAM, and HPL structures is lower compared to hexagonal (HEX) and spherical (SPH) structures. This suggests that, in this system, the self-assembled micelles arranged in HEX or SPH configurations pack more tightly against each other.

Figure 9 and Scheme 1(c) depict phase diagrams of all mesoporous PDDSQ-27 hybrids after template removal,

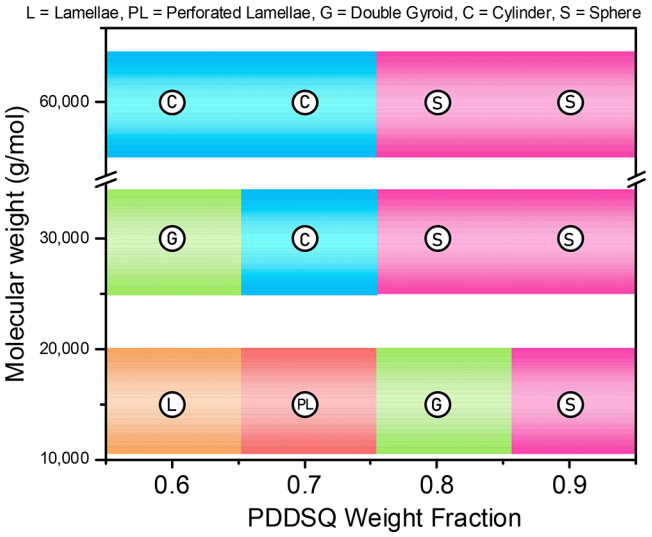


**Figure 9.** Mesoporous structure phase diagram of the PDDSQ-27 hybrid templated from PDDSQ/nEC blends from SAXS and TEM analyses.

illustrating different blending ratios and template molecular weights. Here, two points need to be highlighted. First, it is noticeable that the level of wet-brush behavior affects the phase formation in the PDDSQ-27 blending system. As the chain length enlarges, the $\alpha$ value becomes smaller, and the structure with high interfacial curvature starts to substitute for the low interfacial curvature structure. For example, double gyroid substitutes the lamella from EC to 2EC and cylinder substitutes double gyroid from 2EC to 4EC. From another perspective, as the chain length increases, the self-assembled system would favor the formation of high interfacial structure such as sphere or cylinder; thus, the appearance weight fraction interval of these phases will dominate for the high *N* value templated mesoporous PDDSQ hybrids. Second, a new phase is discovered. So far, for structures that belong to the complex packing window (CWP), only double gyroid is discovered in the PDDSQ-25/EC blending system.[31−37] In this section, we apply the PDDSQ-27 and obtained the double gyroid in both EC and 2EC chain lengths; furthermore, we observe a new phase that has not been seen before in any mesoporous PDDSQ or phenolic materials, hexagonally perforated layer (HPL), whose authenticity is verified by TEM and SAXS. HPL structures are typically metastable, as they may exist at relatively lower energy states but can transition into more stable structural forms, such as the double gyroid structure, over prolonged periods or through annealing processes. However, because the materials in this study underwent thermal treatment for solidification, the mesoporous structure remained stable, preventing such phase transitions. Therefore, achieving a stable HPL structure is a particularly remarkable outcome.

## CONCLUSIONS

Various PEO-*b*-PCL diblock copolymers with the same volume fraction but each block segment with different degrees of polymerization are synthesized via ring-opening polymerization as the templates to prepare mesoporous hybrid materials by blending with PDDSQ. By controlling the weight ratios of the blends, competitive phenomena arise between the OH groups of PDDSQ and the hydrogen bonds between PEO and PCL blend segments. With an increasing template chain length, the proportion of hydrogen bond-affected C═O decreases gradually within the PCL segments. SAXS analysis allows us to observe the phase-separated structures and changes in *d*-spacing after EISA, particularly regarding the enhancement of wet-brush behavior due to increased *N* values leading to phase transitions and the appearance of a double first-order peak in the LAM and CYL mixed structure. Phase transitions caused by changes in surface energy due to melting or curing of components are recorded in the temperature-dependent SAXS overlays. A series of mesoporous PDDSQ hybrids with different structures, including LAM, HPL, DG, HPC, and SPH, are obtained after the high-temperature decomposition of EC templates, all exhibiting high surface areas and pore volumes. Through BET, SAXS, and TEM analyses, we could understand the phase transitions brought about by increasing the degree of polymerization of the template while fixing the blending weight fraction, confirming that increasing *N* values can regulate the degree of wet-brush behavior in the system, thereby preparing self-assembled ordered structures with different interfacial curvatures at the same blending weight fraction. Overall, this work demonstrates a method to obtain mesoporous structures in HPL and DG configurations and explains why changing the degree of polymerization of the block copolymer can induce phase transitions through wet-brush theory and competitive hydrogen bonding phenomena.


https://doi.org/10.1021/acs.macromol.4c00665
Macromolecules 2024, 57, 5958−5970

## ■ ASSOCIATED CONTENT

### Supporting Information

The Supporting Information is available free of charge at https://pubs.acs.org/doi/10.1021/acs.macromol.4c00665.

Characterization methods, molecular weight of nEC diblock copolymers, reaction scheme of PDDSQ hybrids, FITR, GPC, $^{1}H$ and $^{13}C$ NMR spectra of PEO-*b*-PCL diblock copolymers and FTIR spectra of PDDSQ-27 hybrid, FTIR spectra analyses of PDDSQ/nEC blends, and SAXS patterns of PDDSQ/nEC1 blends (PDF)

## ■ AUTHOR INFORMATION


### Corresponding Author

**Shiao-Wei Kuo** − *Department of Materials and Optoelectronic Science, Center for Functional Polymers and Supramolecular Materials, National Sun Yat-Sen University, Kaohsiung 80424, Taiwan;* orcid.org/0000-0002-4306-7171; Email: kuosw@facutly.nsysu.edu.tw

### Author

**Ting-Chih Chou** − *Department of Materials and Optoelectronic Science, Center for Functional Polymers and Supramolecular Materials, National Sun Yat-Sen University, Kaohsiung 80424, Taiwan*

Complete contact information is available at: https://pubs.acs.org/10.1021/acs.macromol.4c00665


### Author Contributions

The manuscript was written through contributions of all authors.

### Notes

The authors declare no competing financial interest.

## ■ ACKNOWLEDGMENTS

This study was supported financially by the National Science and Technology Council, Taiwan, under contracts NSTC 112-2218-E-110-007, and 112-2223-E-110-004. The authors thank the staff at National Sun Yat-sen University for their assistance with the TEM (ID: EM022600) experiments.

## ■ REFERENCES


(1) Lee, S.; Bluemle, M. J.; Bates, F. S. Discovery of a Frank-Kasper $\sigma$ Phase in Sphere-Forming Block Copolymer Melts. *Science* **2010**, *330*, 349−353.

(2) Luo, M.; Epps, T. H. Directed block copolymer thin film self-assembly: emerging trends in nanopattern fabrication. *Macromolecules* **2013**, *46*, 7567−7579.

(3) Liberman-Martin, A. L.; Chu, C. K.; Grubbs, R. H. Application of bottlebrush block copolymers as photonic crystals. *Macromol. Rapid Commun.* **2017**, *38*, 1700058.

(4) Akkineni, S.; Doerk, G. S.; Shi, C.; Jin, B.; Zhang, S.; Habelitz, S.; De yoreo, J. J. Biomimetic Mineral Synthesis by Nanopatterned Supramolecular-Block Copolymer Templates. *Nano Lett.* **2023**, *23*, 4290−4297.

(5) Xiang, Y.; Chuang, W. T.; Chiang, Y. W. Synergistic effects of dry-brush compatibility and shear stress on rapid alignment of lamellar microstructures for block copolymer reflectors. *Giant* **2024**, *17*, 100225.

(6) Warren, S. C.; Messina, L. C.; Slaughter, L. S.; Kamperman, M.; Zhou, Q.; Gruner, S. M.; DiSalvo, F. J.; Wiesner, U. Ordered mesoporous materials from metal nanoparticle−block copolymer self-assembly. *Science* **2008**, *320*, 1748−1752.

(7) Kuo, S. W. Construction Archimedean tiling patterns based on soft materials from block copolymers and covalent organic frameworks. *Giant* **2023**, *15*, 100170.

(8) Huang, Y. S.; Ejeta, D. D.; Kuo, S. W.; Nakamura, Y.; Huang, C. F. Combinations (E) among controlled/living polymerizations and utilizations of efficient chemical reactions for the synthesis of novel polymeric materials. *Polym. Chem.* **2023**, *14*, 4783−4803.

(9) Creutz, S.; Teyssié, P.; Jérôme, R. Living anionic homopolymerization and block copolymerization of (dimethylamino) ethyl methacrylate. *Macromolecules* **1997**, *30*, 6−9.

(10) Wendler, U.; Bohrisch, J.; Jaeger, W.; Rother, G.; Dautzenberg, H. Amphiphilic cationic block copolymers via controlled free radical polymerization. *Macromol. Rapid Commun.* **1998**, *19*, 185−190.

(11) Foster, J. C.; Damron, J. T.; Zhang, H. Simple Monomers for Precise Polymer Functionalization During Ring-Opening Metathesis Polymerization. *Macromolecules* **2023**, *56*, 7931−7938.

(12) Hadjichristidis, N.; Iatrou, H.; Pitsikalis, M.; Mays, J. Macromolecular architectures by living and controlled/living polymerizations. *Prog. Polym. Sci.* **2006**, *31*, 1068−1132.

(13) Winey, K. I.; Thomas, E. L.; Fetters, L. J. The ordered bicontinuous double-diamond morphology in diblock copolymer/homopolymer blends. *Macromolecules* **1992**, *25*, 422−428.

(14) Tanaka, H.; Hasegawa, H.; Hashimoto, T. Ordered structure in mixtures of a block copolymer and homopolymers. 1. Solubilization of low molecular weight homopolymers. *Macromolecules* **1991**, *24*, 240−251.

(15) Hashimoto, T.; Tanaka, H.; Hasegawa, H. Ordered structure in mixtures of a block copolymer and homopolymers. 2. Effects of molecular weights of homopolymers. *Macromolecules* **1990**, *23*, 4378−4386.

(16) Matsen, M. W. Stabilizing new morphologies by blending homopolymer with block copolymer. *Phys. Rew. Lett.* **1995**, *74*, 4225.

(17) Matsen, M. W. Phase behavior of block copolymer/homopolymer blends. *Macromolecules* **1995**, *28*, 5765−5773.

(18) Koizumi, S.; Hasegawa, H.; Hashimoto, T. Ordered structure of block polymer/homopolymer mixtures, 4. Vesicle formation and macrophase separation. *Makromolekulare Chemie. Macromol. Symp.* **1992**, *62*, 75−91.

(19) Lee, H. F.; Kuo, S. W.; Huang, C. F.; Lu, J. S.; Chan, S. C.; Wang, C. F.; Chang, F. C. Hydrogen-bonding interactions mediate the phase behavior of an AB/C block copolymer/homopolymer blend comprising poly (methyl methacrylate-b-vinylpyrrolidone) and poly (vinylphenol). *Macromolecules* **2006**, *39*, 5458−5465.

(20) Chen, W. C.; Kuo, S. W.; Jeng, U. S.; Chang, F. C. Self-assembly through competitive interactions of miscible diblock copolymer/homopolymer blends: Poly (vinylphenol-b-methyl methacrylate)/poly (vinylpyrrolidone) blend. *Macromolecules* **2008**, *41*, 1401−1410.

(21) Tsai, S.-C.; Lin, Y.-C.; Lin, E.-L.; Chiang, Y.-W.; Kuo, S.-W. Hydrogen bonding strength effect on self-assembly supramolecular structures of diblock copolymer/homopolymer blends. *Polym. Chem.* **2016**, *7*, 2395−2409.

(22) Kuo, S.-W. Hydrogen bond-mediated self-assembly and supramolecular structures of diblock copolymer mixtures. *Polym. Int.* **2009**, *58*, 455−464.

(23) Kuo, S. W. Hydrogen bonding mediated self-assembled structures from block copolymer mixtures to mesoporous materials. *Polym. Int.* **2022**, *71*, 393−410.

(24) Dobrosielska, K.; Wakao, S.; Suzuki, J.; Noda, K.; Takano, A.; Matsushita, Y. Effect of homopolymer molecular weight on nano-phase-separated structures of AB block copolymer/C homopolymer blends with hydrogen-bonding interactions. *Macromolecules* **2009**, *42*, 7098−7102.

(25) Meng, Y.; Gu, D.; Zhang, F.; Shi, Y.; Cheng, L.; Feng, D.; Wu, Z.; Chen, Z.; Wan, Y.; Stein, A. A family of highly ordered mesoporous polymer resin and carbon structures from organic−organic self-assembly. *Chem. Mater.* **2006**, *18*, 4447−4464.

(26) Song, L.; Feng, D.; Fredin, N. J.; Yager, K. G.; Jones, R. L.; Wu, Q.; Zhao, D.; Vogt, B. D. Challenges in fabrication of mesoporous

carbon films with ordered cylindrical pores via phenolic oligomer self-assembly with triblock copolymers. *ACS Nano* **2010**, *4*, 189−198.
(27) EL-Mahdy, A. F. M.; Yu, T. C.; Kuo, S. W. Synthesis of Multiple Heteroatom−Doped Mesoporous Carbon/Silica Composites for Supercapacitors. *Chem. Eng. J.* **2021**, *414*, 128796.
(28) EL-Mahdy, A. F. M.; Liu, T.-E.; Kuo, S.-W. Direct synthesis of nitrogen-doped mesoporous carbons from triazine-functionalized resol for $CO_2$ uptake and highly efficient removal of dyes. *J. Hazard. Mater.* **2020**, *391*, 122163.
(29) Mohamed, M. G.; Atayde, E. C., Jr; Matsagar, B. M.; Na, J.; Yamauchi, Y.; Wu, K. C.-W.; Kuo, S.-W. Construction hierarchically mesoporous/microporous materials based on block copolymer and covalent organic framework. *J. Taiwan Inst. Chem. Eng.* **2020**, *112*, 180−192.
(30) Lu, Y. S.; Bastakoti, B. P.; Pramanik, M.; Malgras, V.; Yamauchi, Y.; Kuo, S. W. Direct assembly of mesoporous silica functionalized with polypeptides for efficient dye adsorption. *Chem.—Eur. J.* **2016**, *22*, 1159−1164.
(31) Chen, W. C.; Liu, Y. T.; Kuo, S. W. Mesoporous Organic/Inorganic Hybrid Materials with Frank-Kasper Phases Templated by an Unusual Linear Symmetry Diblock Copolymer. *Macromol. Rapid Commun.* **2021**, *42*, 2100302.
(32) Huang, Y.-C.; Chen, W.-C.; Kuo, S.-W. Mesoporous phenolic/poss hybrids induced by microphase separation arising from competitive hydrogen bonding interactions. *Macromolecules* **2022**, *55*, 8918−8930.
(33) Li, J.-G.; Lin, Y.-D.; Kuo, S.-W. From microphase separation to self-organized mesoporous phenolic resin through competitive hydrogen bonding with double-crystalline diblock copolymers of poly (ethylene oxide-b-ε-caprolactone). *Macromolecules* **2011**, *44*, 9295−9309.
(34) Li, J. G.; Ho, Y. F.; Ahmed, M. M.; Liang, H. C.; Kuo, S. W. Mesoporous carbons templated by PEO-PCL block copolymers as electrode materials for supercapacitors. *Chem.—Eur. J.* **2019**, *25*, 10456−10463.
(35) Chen, W.-C.; Kuo, S.-W. Ortho-imide and allyl groups effect on highly thermally stable polybenzoxazine/double-decker-shaped polyhedral silsesquioxane hybrids. *Macromolecules* **2018**, *51*, 9602−9612.
(36) Chen, W.-C.; Liu, Y.-T.; Kuo, S.-W. Highly thermal stable phenolic resin based on double-decker-shaped POSS nanocomposites for supercapacitors. *Polymers* **2020**, *12*, 2151.
(37) Kuo, S.-W.; Lin, C.-L.; Chang, F.-C. Phase behavior and hydrogen bonding in ternary polymer blends of phenolic resin/poly (ethylene oxide)/poly (ε-caprolactone). *Macromolecules* **2002**, *35*, 278−285.
(38) Kuo, S.-W. Hydrogen-bonding in polymer blends. *J. Polym. Res.* **2008**, *15*, 459−486.
(39) Kuo, S.-W. *Hydrogen Bonding in Polymeric Materials*; Wiley VCH, 2018; DOI: DOI: 10.1002/9783527804276.
(40) Kuo, S.-W. Hydrogen bonding interactions in polymer/polyhedral oligomeric silsesquioxane nanomaterials. *J. Polym. Res.* **2022**, *29*, 69.
(41) Drolet, F.; Fredrickson, G. H. Combinatorial screening of complex block copolymer assembly with self-consistent field theory. *Phys. Rev. Lett.* **1999**, *83*, 4317.
(42) Müller, M.; Schmid, F. Incorporating fluctuations and dynamics in self-consistent field theories for polymer blends. *Advanced Computer Simulation Approaches for Soft Matter Sciences II* **2005**, *185*, 1−58.
(43) Tyler, C. A.; Qin, J.; Bates, F. S.; Morse, D. C. SCFT study of nonfrustrated ABC triblock copolymer melts. *Macromolecules* **2007**, *40*, 4654−4668.
(44) Hu, D.; Zheng, S. Reaction-induced microphase separation in epoxy resin containing polystyrene-block-poly (ethylene oxide) alternating multiblock copolymer. *Eur. Polym. J.* **2009**, *45*, 3326.
(45) Yu, R.; Zheng, S.; Li, X.; Wang, J. Reaction-induced microphase separation in epoxy thermosets containing block copolymers composed of polystyrene and poly (ε-caprolactone): Influence of copolymer architectures on formation of nanophases. *Macromolecules* **2012**, *45*, 9155.
(46) Xu, Z.; Zheng, S. Reaction-induced microphase separation in epoxy thermosets containing poly (ε-caprolactone)-block-poly (n butyl acrylate) diblock copolymer. *Macromolecules* **2007**, *40*, 2548.
(47) Li, J. G.; Chu, W. C.; Jeng, U. S.; Kuo, S. W. In Situ Monitoring of the Reaction-Induced Self-Assembly of Phenolic Resin Templated by Diblock Copolymers. *Macromol. Chem. Phsy.* **2013**, *214*, 2115−2123.
(48) Hsueh, H.-Y.; Chen, H.-Y.; She, M.-S.; Chen, C.-K.; Ho, R.-M.; Gwo, S.; Hasegawa, H.; Thomas, E. L. Inorganic gyroid with exceptionally low refractive index from block copolymer templating. *Nano Lett.* **2010**, *10*, 4994−5000.
(49) Sakurai, S.; Isobe, D.; Okamoto, S.; Yao, T.; Nomura, S. Collapse of the Ia $3^-$ d cubic symmetry by uniaxial stretching of a double-gyroid block copolymer. *Phys. Rev. E* **2001**, *63* (6), 061803.
(50) Bates, F. S.; Schulz, M. F.; Khandpur, A. K.; Förster, S.; Rosedale, J. H.; Almdal, K.; Mortensen, K. Fluctuations, conformational asymmetry and block copolymer phase behaviour. *Farad. Disc.* **1994**, *98*, 7−18.
(51) Khandpur, A. K.; Foerster, S.; Bates, F. S.; Hamley, I. W.; Ryan, A. J.; Bras, W.; Almdal, K.; Mortensen, K. Polyisoprene-polystyrene diblock copolymer phase diagram near the order-disorder transition. *Macromolecules* **1995**, *28*, 8796−8806.
(52) Hajduk, D. A.; Takenouchi, H.; Hillmyer, M. A.; Bates, F. S.; Vigild, M. E.; Almdal, K. Stability of the perforated layer (PL) phase in diblock copolymer melts. *Macromolecules* **1997**, *30*, 3788−3795.




https://doi.org/10.1021/acs.macromol.4c00665
*Macromolecules* 2024, 57, 5958−5970